

OPEN ACCESS

EDITED BY Hao Wang.

North China University of Science and Technology, China

REVIEWED BY

Xuepeng Song,

Jiangxi University of Science and Technology, China

Rui Gao

Taiyuan University of Technology, China Sheng Zhang,

Central South University, China Wenyue Qi,

Yanshan University, China

*CORRESPONDENCE

Hengfeng Liu,

⋈ hengfengliu@cumt.edu.cn

Xiao Wang,

⊠ x.wang@xzit.edu.cn

RECEIVED 10 October 2025 REVISED 01 November 2025 ACCEPTED 03 November 2025 PUBLISHED 18 November 2025

CITATION

Liu H, Guo J, Rodriguez-Dono A, Topal E, Feng J, Li X, Wang X and Zhao H (2025) Study on the flow and diffusion behavior of coal gangue slurry in subsequent space after mining: physical and numerical simulation. *Front. Environ. Sci.* 13:1722548. doi: 10.3389/fenvs.2025.1722548

COPYRIGHT

© 2025 Liu, Guo, Rodriguez-Dono, Topal, Feng, Li, Wang and Zhao. This is an open-access article distributed under the terms of the Creative Commons Attribution License (CC BY). The use, distribution or reproduction in other forums is permitted, provided the original author(s) and the copyright owner(s) are credited and that the original publication in this journal is cited, in accordance with accepted academic practice. No use, distribution or reproduction is permitted which does not comply with these terms.

Study on the flow and diffusion behavior of coal gangue slurry in subsequent space after mining: physical and numerical simulation

Hengfeng Liu^{1*}, Jiahao Guo¹, Alfonso Rodriguez-Dono², Erkan Topal³, Jianye Feng⁴, Xinying Li¹, Xiao Wang^{5*} and Heng Zhao⁶

¹School of Mines, China University of Mining and Technology, Xuzhou, China, ²Department of Graphic and Design Engineering, Universitat Politècnica de Catalunya, Barcelona, Spain, ³WA School of Mines: Minerals, Energy and Chemical Engineering, Curtin University, Perth, WA, Australia, ⁴Key Laboratory of Xinjiang Coal Resources Green Mining, Ministry of Education, Xinjiang Institute of Engineering, Urumqi, China, ⁵School of Environmental Engineering, Xuzhou University of Technology, Xuzhou, China, ⁶Jiangsu Design Institute of Geology for Mineral Resources (Testing Center of China National Administration of Coal Geology), Xuzhou, China

The application of grouting backfill technology in the Subsequent Space after Mining (SSM) in coal mines effectively addresses the dual challenges of coalbased solid waste disposal and surface subsidence control. However, the SSM, often likened to a geological "black box," is difficult to visualize, which severely hinders the widespread application of this technology. This study overcomes this challenge by using a self-developed two-dimensional visual physical simulation system for sealed grouting in the SSM, which has been validated through numerical simulation. This system enables visualization and precise quantitative analysis of the flow and diffusion behavior of coal gangue slurry within the SSM. The results indicate that as the working face advances, the SSM undergoes a dynamic evolution involving fracture development, separation layer formation, and eventual roof collapse. This process leads to a maximum roof subsidence of 5.51 m and the formation of 16 stable fracture zones. Among these, the fracture network formed by zones $T_7^{\#}$ to $T_{10}^{\#}$ and $L_1^{\#}$ to $L_6^{\#}$ serves as the key SSM for slurry accommodation and effective backfilling. The spread of the coal gangue slurry is primarily controlled by the connectivity of the fracture network, demonstrating notable spatiotemporal variation. In fractures $T_1^{\#}$ to $T_6^{\#}$, the slurry exhibits an "oval-spindle" diffusion morphology with a gradually declining flow rate over time. In contrast, within fractures $T_7^{\#}$ to $T_{10}^{\#}$ and $L_1^{\#}$ to $L_6^{\#}$, the slurry migrates in a "top-to-bottom" and "right-to-left" pattern without a reduction in diffusion rate. Furthermore, the grouting horizon is identified as the most influential factor on the slurry's diffusion range, followed by grouting pressure, while slurry concentration has the least impact. The optimal levels for the three factors—grouting pressure, grouting layer, and slurry concentration—are Level 3 (0.8 MPa), Level 3 ($T_1^{\#}$ - $T_{10}^{\#}$, $L_1^{\#}$ - $L_6^{\#}$), and Level 1 (60%), respectively.

KEYWORDS

coal gangue slurry, grouting backfilling, fracture network, subsidence control, ecological restoration

1 Introduction

Coal has long served as the cornerstone of China's energy structure and a fundamental guarantee of its energy security; however, large-scale mining activities have triggered significant resource waste and environmental damage. On the one hand, the coal mining process yields substantial quantities of coal-based solid waste: coal gangue alone accounts for about 10%-15% of annual coal output, with accumulated stockpiles exceeding 7 billion tons and an annual growth of approximately 150 million tons (Yi et al., 2023). In 2024, coal gangue output reached 717 million tons (Tang et al., 2024), yet its comprehensive utilization rate remains below 70% (Li and Wang, 2019; Gao et al., 2021). Meanwhile, associated solid wastes such as fly ash continue to accumulate, with China's annual fly ash production surpassing 600 million tons and a utilization rate of around 80% (Zhang et al., 2023). Long-term stockpiling also raises safety concerns including spontaneous ignition and landslides, in addition to aggravating atmospheric and water pollution (Lazorenko and Kasprzhitskii, 2025; Amiri et al., 2022). Conventional approaches to utilizing coal-based solid waste-such as power generation, building material production, and landfilling-are further constrained by high energy consumption, logistical challenges, and limited disposal capacity (Taha et al., 2017; Karimaei et al., 2020; Snehasree et al., 2025). On the other hand, mining operations have induced severe surface subsidence and land degradation. Estimates indicate that underground mining in China results in a subsidence area of 0.20-0.33 ha per 10,000 tons of extracted coal, and in 2022 alone, newly formed subsidence zones reached 76,500-126,200 ha, posing serious threats to ecological security and regional sustainable development (Li, 2023). In response, backfill mining methods have been developed. However, existing underground backfill techniques, while capable of processing some solid waste, often suffer from "mining-backfill interference," which impedes mining efficiency and fails to make full use of the fracture networks formed in the overlying strata (Song et al., 2022). Against this backdrop, grouting backfill technology in the SSM has emerged. By injecting slurry made from coal-based waste into the SSM in a targeted and efficient manner, this approach achieves the dual objectives of large-scale solid waste disposal and effective surface subsidence control, positioning itself as a key research direction for green mining in the coal industry.

Scholars worldwide have conducted extensive research on the structural evolution of the SSM and the flow and diffusion mechanisms of grouting slurry. Regarding the structural evolution of SSM, Wang et al. (2004) employed threedimensional physical similarity simulation to investigate the fracture development and breakage patterns of overlying strata in shallow coal seams. Their findings revealed that under full extraction conditions, the fracture arch height is approximately half the mining length. Roof breakage was more pronounced along the mining direction, evolving from symmetric to asymmetric, ultimately forming a tetrahedral shape in the broken space. Yavuz (2004) investigated the structural evolution of overburden pressure recovery distance and stress distribution in longwall coal mine goafs through theoretical modeling and numerical simulation methods. The study found that the overburden pressure recovery distance increases exponentially with mining depth and is influenced by mining height, bulking factor, and rock strength, while the stress distribution follows an S-shaped curve. Ghabraie et al. (2015) employed physical modeling with sand-plaster similitude materials and numerical simulations to study the structural evolution of goafs induced by sequentially extracted partially overlapping longwall panels. Their research revealed that the goaf can be divided into three regions with distinct movement characteristics after lower-seam mining, with significantly enhanced subsidence in the overlapping area and an asymmetrical distribution of limit angles. Xu et al. (2020) systematically studied the spatial distribution characteristics of overburden failure through theoretical analysis and laboratory experiments. They discovered a critical movement interface in the overlying strata of shallow coal seam subsequent spaces, which causes opposing horizontal movement patterns in the strata above and below the interface, leading to skewed subsidence and interlayer dislocation of the overburden. Li et al. (2020) analyzed the influence of compression deformation of deep backfill materials (e.g., gangue) on strata movement and the fracture evolution of key layers using similarity simulation. Their results showed that the fracture of key layers creates a continuous fracture network distributed on both sides and the middle-lower part of the subsequent space, thereby dominating the structural evolution of the SSM. Sahoo et al. (2020) conducted a plane-strain numerical simulation based on FLAC 2D and developed FISH subroutines to investigate the progressive compaction and structural evolution of goafs in pillarless depillaring mining. The study showed that the goaf material experiences a 15% stress recovery after the main collapse, with stress recovery reaching 89% as the working face advances to 200 m, and the stress distribution exhibits a concave profile with the maximum stress point shifting toward the working face. Kostecki and Spearing (2015) utilized FLAC3D numerical simulation to study the influence of backfill materials on the collaborative load-bearing behavior of a coal pillar-floor system with a weak floor. Their research demonstrated that backfill materials promote the formation of a cooperative load-bearing structure by suppressing shear failure in coal pillars, consequently influencing the evolutionary characteristics of the SSM structure. Sepehri et al. (2017) analyzed the stress distribution in surrounding rock and surface subsidence induced by diamond mining using 3D elastoplastic finite element simulation. Their study found that the induced subsidence profile follows a Gaussian distribution, with a significant increase (approximately 44%) in settlement magnitude as mining approaches the surface. Khanal et al. (2016) employed COSFLOW numerical simulation to study the impact of different layouts in multi-seam mining on surface subsidence and chain pillar stress. Their results indicated that the mining direction has a limited effect on subsidence control, whereas the layout of the top panel dominates the surface subsidence profile morphology. Ghabraie et al. (2017) investigated the structural evolution of the SSM induced by multi-seam longwall mining based on finite element numerical simulation. They found that their proposed layered damage model could accurately simulate rock mass failure propagation, subsequent space re-collapse, and stress transfer processes, thereby revealing the mechanisms of overburden structural evolution and enhanced surface subsidence under multi-stage mining.

On the grouting slurry diffusion mechanisms, Wang et al. (2021) established a theoretical model correlating grouting parameters with

surface subsidence. Their study found that slurry diffuses in an elliptic paraboloid shape within separated overburden strata, and the subsidence reduction efficiency follows a three-stage "slow-fastslow" growth pattern as the grouting-to-mining ratio increases. Zhou et al. (2025) numerically simulated the flow and diffusion behavior of coal gangue slurry in mined-out spaces. They demonstrated that by controlling grouting pressure and the grouting-to-mining ratio, slurry can effectively diffuse into separation zones beneath key strata and form a uniform supporting body, thereby significantly controlling surface subsidence. Yu et al. (2021) employed discrete element modeling to investigate slurry diffusion in soft coal seams. Their results showed that grouting progresses through stages of seepage, rapid fracturing, slow fracturing, and stabilization, with pre-existing fractures significantly increasing the slurry diffusion radius. Bouchelaghem and Vulliet (2001) combined theoretical analysis with laboratory experiments to study slurry diffusion in saturated porous media. They found that slurry diffusion is jointly controlled by convective transport, hydrodynamic dispersion, and particle adsorption/filtration. Pedrotti et al. (2017) integrated experimental testing with theoretical modeling to examine slurry diffusion capacity, establishing that slurry diffusion follows a "timedependent viscosity" law, where initially low viscosity enables longdistance permeation. Zhang et al. (2018) conducted model tests and PFC2D numerical simulations to study slurry diffusion in loess. Their research revealed that fracture grouting in loess involves stages of compaction and fracturing under pressure, ultimately forming a "Y"-shaped slurry vein controlled by maximum shear stress. Zheng et al. (2021), Zheng et al. (2025) used DEM software to analyze the diffusion range and pressure distribution of cement slurry during grouting. They found that in soil-rock mixtures, slurry primarily diffuses by forming heterogeneous, multi-branched fracture veins, and more uniformly distributed veins result in lower macroscopic strength of the formed support skeleton. El Tani and Stille (2017) investigated the diffusion behavior of silicate solutions and cementbased grouts in rock fractures through theoretical analysis, finding that the grout diffusion process is governed by constant flow rate, pressure, or energy during injection. They emphasized the need to define stopping criteria based on the diffusion-time relationship to optimize grouting effectiveness. El Mohtar et al. (2022) studied the diffusion patterns of fine cement grouts in permeation grouting using digital imaging experiments. Their research revealed that grout stability significantly influences diffusion uniformity, with unstable grouts prone to filtration, leading to uneven concentration distribution and deviations of the propagation front from theoretical predictions. Mohajerani et al. (2017) developed a two-dimensional numerical model based on the Explicit Grout Forehead Pressure algorithm to examine grout diffusion in fracture networks. They found that the presence of pore fluids substantially reduces the grout's diffusion range, while the time-dependent hardening characteristics and initial yield stress of the grout are critical factors affecting its diffusion efficiency. Güllü (2016) conducted a study aimed at comparing the most common rheological models used for jet grout mixtures, which are generated due to the addition of stabilizers (such as clay, sand, lime, and bottom slurry). The research findings show that among the relevant rheological models, the Robertson-Stiff and derived ones within high ranking, De Kee, Herschel-Bulkley and Modified Bingham within moderate ranking, and Bingham, Herschel-Bulkley and Modified Bingham within low ranking. Heever et al. (2014) in their analysis of homogeneous non-Newtonian fluid pipe flow, demonstrated that the prediction of laminar flow pressure gradients is insensitive to the rheological model, but the transition velocity and turbulence predictions are significantly influenced by the model, with the Casson model consistently performing well in turbulence predictions. Letelier et al. (2023) in their study on the flow of viscoelastic fluids (Bingham and Herschel-Bulkley fluids) in non-circular pipes, revealed the influence of the power-law index and Bingham number on the morphology of plug flow and stagnant regions. Qu et al. (2022) in their investigation of the rheological properties of semi-solid slurries, found that the power-law model under controlled shear stress is more suitable for die-casting filling simulations.

In summary, although significant progress has been made in existing research on the evolution of SSM structures and the flow and diffusion laws of grouting slurry, a critical research gap remains: there are few reports on visualized two-dimensional physical models for sealed grouting and filling in SSM, which hinders the accurate acquisition and analysis of the real flow and diffusion behavior of coal gangue slurry in the SSM. To address this gap, this study aims to bridge this research void, with its core novelty and main contributions reflected in the following three aspects: (1) A visualized two-dimensional physical simulation system for sealed grouting backfilling in SSM was constructed, enabling the visual observation and precise quantitative analysis of the entire process of coal gangue slurry flow and diffusion in the SSM (2) By coupling physical simulation with numerical simulation, mutual validation of the two methods was achieved, significantly enhancing the reliability and universality of the research conclusions. (3) The two key processes "overlying strata movement SSM structure evolution" and "spatiotemporal patterns of slurry flow and diffusion" were systematically integrated, comprehensively revealing the dynamic behavior of slurry flow and diffusion in SSM. The research findings provide a theoretical basis and technical guidance for green coal mining and the resource utilization of coal-based solid waste.

2 Materials and methods

2.1 Material performance analysis

2.1.1 Physical and chemical properties of raw materials

A typical mine located within the jurisdictions of Zhasak Town and Hongqinghe Town, with the initial mining and filling coal face designated as 1303N-1#. The coal seam is No. 3, exhibiting a thickness ranging from 2.2 to 3.63 m, with an average thickness of 3.19 m. The seam inclination measures between 9 and 13°, averaging 11°. Test coal gangue samples were extracted from the Yungang Coal Mine in Datong City, Shanxi Province, China.

2.1.1.1 Mineral composition

The mineral composition of gangue from Yungang Coal Mine was analyzed using X-ray diffraction. The results indicate that the primary minerals are quartz (45.85%), kaolinite (30.50%), and muscovite (15.65%). Quartz is the main component of sandstone,

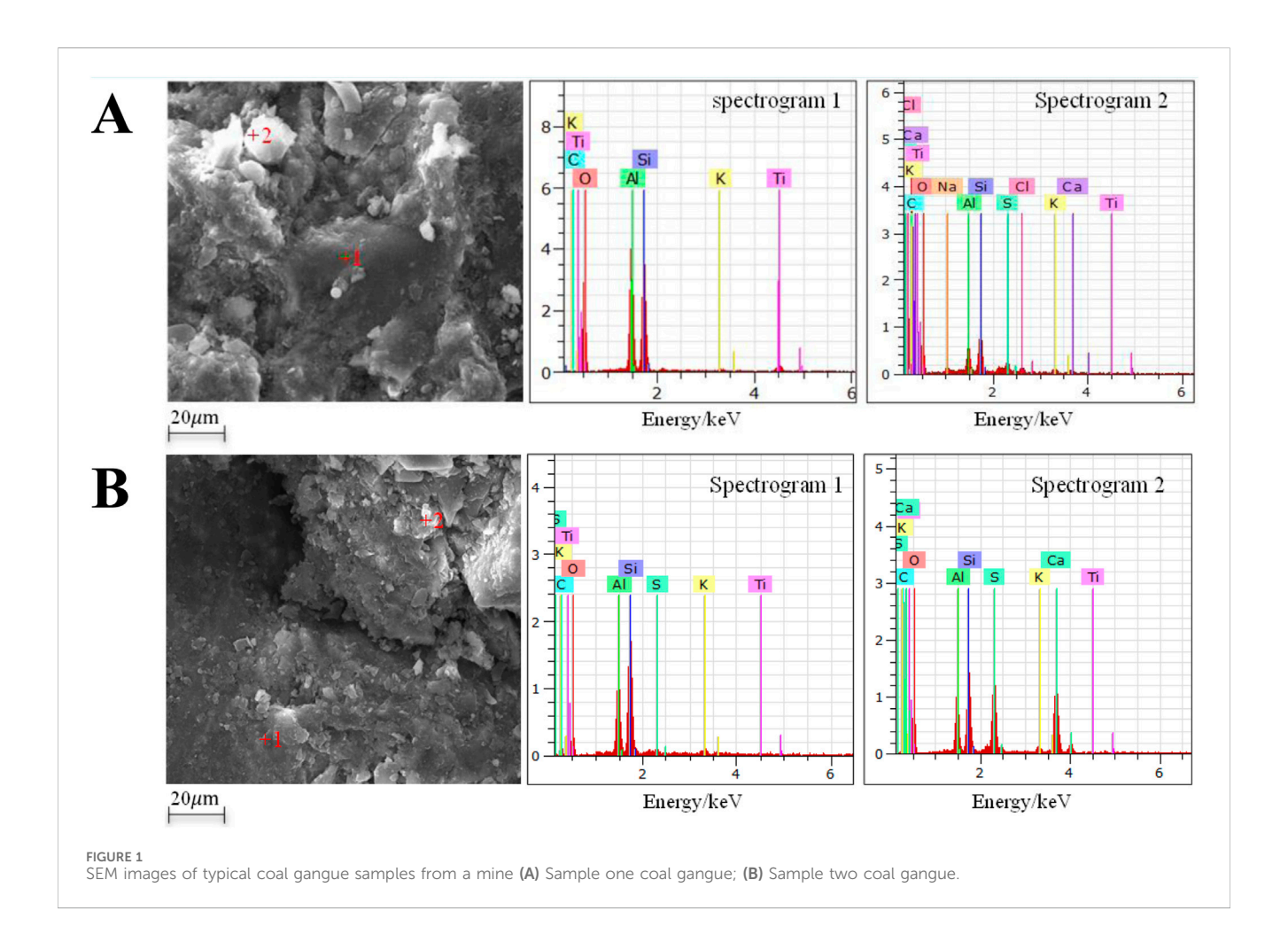


TABLE 1 Testing protocol for rheological properties of coal gangue slurry.

Scheme Number	1	2	3	4	5	6	7	8	9
Slurry concentration/%	60	60	60	65	70	65	65	70	70
Fine aggregate content/%	55	60	66	55	55	60	66	60	66
Coarse aggregate content/%	45	40	34	45	45	40	34	40	34

while kaolinite and muscovite are key constituents of mudstone. This demonstrates that the gangue sampled from the Yungang Coal Mine consists predominantly of sandstone and mudstone, which is consistent with the lithology of the roof and floor strata of the mined coal seam.

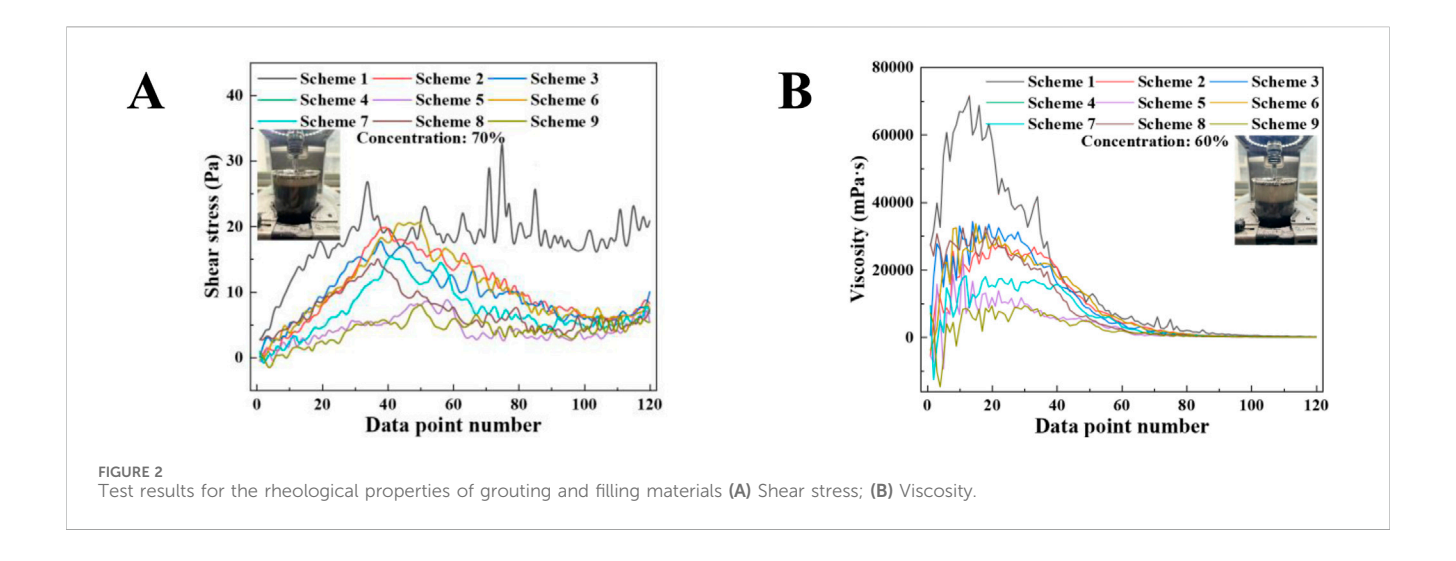
2.1.1.2 Detailed structural analysis

The meso-morphology and elemental composition of gangue from a typical coal mine were characterized using scanning electron microscopy (SEM), with results shown in Figure 1. The gangue sample consists primarily of a clay mineral matrix embedded with quartz and potassium-containing clay minerals. The matrix is predominantly composed of irregularly shaped, black clay minerals, with energy-dispersive spectroscopy (EDS) analysis revealing a significant carbon content in these areas. Embedded

within this matrix are numerous mineral particles of varying sizes and morphologies: bright white, angular particles identified by EDS as quartz; regions exhibiting distinct sheet-like cleavage structures with primary elemental compositions of aluminum, silicon, and potassium, confirming the presence of clay minerals; and pore areas showing concentrated distributions of chlorine, sodium, calcium, and sulfur elements, indicating crystallization of minerals such as gypsum. Furthermore, well-developed micro-fissures were observed, with some fissure widths measuring less than 1 μm .

2.1.2 Rheological properties of coal gangue slurry

This study systematically investigated the rheological properties of coal gangue slurry under varying mix ratios and solid concentrations. The experimental procedure primarily comprised the following steps: (1) The raw coal gangue slurry is first processed



through a jaw crusher to break large chunks into particles suitable for subsequent treatment, ensuring material uniformity and enhancing screening efficiency. (2) The crushed coal gangue slurry was sieved to separate fine aggregate (particle size <0.25 mm) from coarse aggregate (particle size 0.25-5 mm). The screening process aimed to precisely control the particle size distribution, providing a basis for the subsequent slurry proportioning design. (3) According to the nine experimental schemes outlined in Table 1, corresponding masses of fine and coarse aggregates were weighed based on the designated ratios and slurry concentrations, then uniformly mixed with water. During preparation, mechanical stirring was applied to ensure thorough blending, forming a homogeneous slurry and preventing particle sedimentation or local concentration variations that could affect test results. (4) The rheological properties of the slurry were measured using an SDL580SS rotational rheometer (torque accuracy ±0.5% FS, strain accuracy ±1%, speed accuracy ±0.5%). During testing, the shear rate was increased stepwise according to preset values, while shear stress and viscosity were recorded in real time. A brief stabilization period was maintained at each shear rate step to accurately capture the transition of the slurry from a static state to a fully sheared condition. Data points were numbered in accordance with the loading sequence to facilitate analysis of rheological behavior evolution. The test results are presented in Figure 2.

The study revealed distinct trends in shear stress as a function of shear rate for different proportions of fine aggregate, coarse aggregate, and coal gangue slurry concentrations. When the mixture consisted of 55% fine aggregate, 45% coarse aggregate, and a slurry concentration of 60%, the shear stress increased significantly with rising shear rate. Under other mix proportions, however, the stress growth remained relatively gradual in the low shear rate region but escalated sharply at higher shear rates. This behavior indicates that the coal gangue slurry exhibits strong structural stability in the low-speed region, whereas at higher speeds, its internal structure becomes progressively disrupted, and interparticle forces weaken. As a result, the slurry transitions from a solid-like to a fluid-like state. These findings demonstrate that variations in mix proportion and concentration directly alter the particle packing morphology and flocculation characteristics of

the coal gangue slurry, thereby influencing its resistance to shear deformation.

Viscosity reflects the internal friction and interparticle interactions within the coal gangue slurry, is significantly influenced by aggregate gradation and slurry concentration. As the slurry concentration increased from 60% to 70%, the viscosity rose markedly, enhancing interparticle friction and flocculation effects, which in turn reduced fluidity. At a fixed concentration, a higher proportion of fine aggregate also led to increased viscosity, attributable to the fine particles filling the voids between coarse particles and forming a denser slurry skeleton. Therefore, the viscosity of coal gangue slurry not only governs its flow performance but also directly affects its seepage characteristics in porous media. According to relevant permeability theory, the permeability coefficient Kg is inversely proportional to the viscosity μ , as expressed by the following Equation 1 (Wang et al., 2024):

$$K_g = \frac{\gamma_b k}{1} \tag{1}$$

Where, K_g represents the permeability coefficient (m/s), γ_b represents the unit weight of the coal gangue slurry (kg/m³), k represents the intrinsic permeability of the medium, and μ represents the viscosity of the coal gangue slurry (Pa·s). This indicates that an increase in viscosity leads to a reduction in the permeability coefficient of the slurry, thereby weakening its ability to diffuse and permeate through fractures and pores. In the subsequent numerical simulations conducted in this study, viscosity data obtained from rheological tests on the coal gangue slurry were used to assign and calibrate the fluid viscosity and related seepage parameters in the model. This approach ensures that the simulation results accurately represent the seepage and diffusion characteristics of the coal gangue slurry within the SSM.

In summary, the rheological properties of coal gangue slurry are jointly influenced by the proportion of fine and coarse aggregates as well as the slurry concentration. Higher concentrations and a greater proportion of fine aggregates significantly increase the viscosity and shear stress of the slurry, enhancing its shear resistance while simultaneously increasing pumping resistance and energy consumption. Moreover, the structural evolution of the coal gangue slurry across different shear stages indicates that the



FIGURE 3

Photograph of the visualized two-dimensional physical simulation system for sealed grouting backfilling in the SSM.

packing and flocculation state of internal particles govern the variation in its flow behavior. Additionally, the rheological characteristics of coal gangue slurry not only determine its mixing and transport properties but also directly affect its seepage and diffusion behavior in porous media.

2.2 Experimental system and methodology for 2D visualized physical simulation of sealed grouting backfilling in the SSM

2.2.1 Description of the experimental system

To investigate the flow and diffusion behavior of coal gangue slurry within the SSM during coal extraction, this study developed a visualized two-dimensional physical simulation system for sealed grouting backfilling in SSM (Figure 3). The experimental setup consists of three main components: a model frame, grouting and loading devices, and a monitoring system.

- The model frame utilizes a steel (Q235) structure as the loadbearing platform, with sealed transparent airbags installed on the front and rear sides to confine the slurry and allow visual observation of its diffusion process. The interior of the frame is layered with similitude materials (such as quartz sand, cement, gypsum, and mica powder), compacted according to similarity theory to simulate coal and rock strata.
- 2. The grouting and loading assembly comprise a pneumatic pump (YZ-KYJ, capacity 50L, rotational speed 3,180 r/min), grouting pump (ZBQ27/1.5, grouting pressure 3.2 MPa, gas consumption 0.5 m³/min), slurry delivery pipelines, and sealed transparent airbags. The pneumatic pump supplies power to the grouting pump, which allows for the regulation of grouting pressure and flow rate. The slurry pipelines are designed to simulate field drilling and grouting processes, replicating the actual engineering

- conditions of slurry injection into the SSM. The sealed transparent airbags, which confine the slurry while allowing visual observation, are fabricated from polyvinyl chloride (PVC) film with a thickness of 0.8 mm. This material exhibits high transparency (light transmittance >90%), good flexibility (elongation at break >250%), and sufficient tensile strength (>15 MPa). The airbags are custom-made and heat-sealed along the edges to ensure leak-proof performance. They are designed to withstand the internal grouting pressures used in the experiments (up to 0.8 MPa) without significant deformation or rupture, thereby maintaining the sealing integrity of the system during grouting.
- 3. The monitoring system includes a MatchID-2D non-contact strain measurement device (Wide measurement range, supporting 0.005%-2000% strain). This digital image correlation system is capable of recording the deformation field of the overlying strata. Using the digital image fixed-point capture analysis method, the deformation of the physical model and the development of fractures are synchronously monitored. Through strain field analysis by the MatchID-2D DIC system, high tensile strain zones were identified and traced, with their outlines digitized to ensure the fracture network accurately represents the key structures from the physical simulation. Deformation monitoring is conducted at 10-minute intervals, while fracture analysis involves collecting 8 photos every 10 min for quantitative evaluation. During the grouting process, the development of the slurry within the fracture network is continuously monitored.

The testing procedure was conducted in two distinct phases. The first phase involved mining simulation, where the working face was progressively advanced to induce initial and periodic roof weighting. This process led to the development of fractures, ruptures, and separation layers within the overlying strata. The primary objective of this phase was to generate a SSM structure representative of actual

10 3389/fenvs 2025 1722548 Liu et al.

	Project Parameters		Project	Parameters		
	Model length	1.4 m	Stress ratio	333.4:1		
Model thickness 0.15 m		0.15 m	Excavation height	2.9 cm		
Model height 1.45 m		1.45 m	Model boundary (boundary coal pillar)	25 cm		

Excavation steps

Single Excavation distance

TABLE 2 Basic parameters table for physical similarity models.

mining conditions. The second phase focused on grouting simulation, during which grouting backfilling was performed within the SSM formed by the mining activity. Throughout both the mining and grouting simulations, the transport characteristics of the coal gangue slurry within the SSM were monitored and recorded. Key parameters included the diffusion range, diffusion pattern, and interactions with overburden deformation.

200:1

1.667:1

2.2.2 Experimental protocol design

Geometric ratio

Bulk density ratio

Based on the mining geological conditions of a typical mine and similarity theory, the geometric ratio of the similar material simulation test model was determined as 200:1, the unit weight ratio as 1.667:1, and the similarity ratio of motion time as 14:1. Consequently, the basic parameters of the physical similarity model and the material ratio parameters for the similar simulation experiment of the typical mine were calculated, as shown in Tables 2, 3.

2.3 Numerical simulation method for coal gangue grouting backfilling in the SSM

2.3.1 Construction of numerical models

To accurately investigate the flow and diffusion behavior of coal gangue slurry in the SSM during coal extraction, a numerical simulation model was developed using COMSOL Multiphysics 6.2 software, based on the results of the physical model tests. The numerical model dimensions are consistent with those of the physical model. Based on the digitized contour results of the physical model obtained through the MatchID-2D DIC system, fracture networks were constructed within the numerical model. This ensured the numerical fracture network could accurately reproduce the key structural features observed in the physical simulation, ultimately forming 16 discrete fracture zones as depicted in Figure 4. The model comprises a total of 232,809 elements, with a simulation time step of 1 s and a total simulation time of 30 s.

The multiphysics coupling model was established using the Transport of Diluted Species in Porous Media (TDS) and Darcy's Law (DL) modules, incorporating the following key assumptions and boundary conditions: The fracture network within the SSM was considered rigid with negligible wall deformation during grouting; and laminar flow conditions were presumed dominant within the fracture channels. A pressure-inlet boundary condition, matching the experimental grouting pressures of respective schemes, was applied at the injection borehole, while pressure-outlet boundaries at atmospheric pressure were assigned to fracture network exits connecting to model boundaries. The fluid was characterized by its density and experimentally determined rheological parameters. This framework enabled the development of a realistic multiphysics model where slurry transport is governed by the convection-dispersion equation, expressed as follows in Equation 2:

$$\frac{\partial}{\partial t} (\theta c_i) + \nabla (\mu c - D_{e,i} \nabla c) = S(X, t)$$
 (2)

18

Where, c represents the solute concentration in the liquid phase (mg/L), θ represents the porosity, μ represents the Darcy velocity (m/s), $D_{e,i}$ represents the effective diffusion coefficient (m²/s), and S_i represents the source term.

The relationship between the seepage velocity and the pressure gradient is given by Darcy's Law, expressed as follows in Equation 3:

$$u = -\frac{k}{\lambda} \nabla p \tag{3}$$

Where, *u* represents the filtration velocity (m/s), λ represents the slurry viscosity (Pa·s), and p is the pressure field (Pa). The Darcy's Law module combines Darcy's law and the continuity equation, expressed as follows in Equation 4:

$$\nabla u = q(\mathbf{X}, t) \tag{4}$$

Where, q (X, t) represents the volumetric source term.

2.3.2 Design of the simulation solution

The accuracy of the numerical model for grouting backfilling was validated using results from physical model tests. Following successful validation, numerical simulation analysis was conducted. To investigate the flow and diffusion behavior of coal gangue slurry, three influencing factors were selected as experimental variables: grouting pressure, grouting horizon, and slurry concentration. Each factor was assigned three levels, and an L9 (33) orthogonal array was employed to design the numerical simulation scheme for grouting backfilling in the SSM. This series comprised a total of nine simulation schemes, with specific details provided in Table 4.

3 Results and analysis

3.1 Overlying strata movement and the SSM structural evolution in coal seam mining

During the working face advancement, the roof behind the excavated area loses support after coal extraction, leading to the initiation of micro-fractures. As mining progresses, these fractures progressively develop into interconnected fractures, separation

TABLE 3 Typical mine similarity simulation experiment material mixing ratio parameters.

No.	Lithology	Mix ratio	Thickness/ m	Model thickness/ cm	Cumulative model Thickness/ cm	Total dry weight/kg	Sand /kg	Lime/kg	Gypsum /kg	Water /kg
1	Medium- grained sandstone	355	39.8	19.9	207.9	80.24	60.18	10.03	10.03	11.46
2	Sandy mudstone	673	18.9	9.5	188.0	38.10	32.66	3.81	1.63	4.23
3	Medium- grained sandstone	355	6.2	3.1	178.6	12.50	9.37	1.56	1.56	1.79
4	Coarse-grained sandstone	437	20.1	10.1	175.5	40.52	32.42	2.43	5.67	4.50
5	Siltstone	737	12.7	6.4	165.4	25.60	22.40	0.96	2.24	2.84
6	Fine-grained sandstone	455	41.2	20.6	159.1	83.06	66.45	8.31	8.31	9.23
7	Medium conglomerate	373	23.7	11.9	138.5	47.78	40.95	3.41	3.41	6.83
8	Fine-grained sandstone	455	17.8	8.9	126.6	35.88	28.71	3.59	3.59	3.99
9	Siltstone	737	35	17.5	117.7	70.56	61.74	2.65	6.17	7.84
10	Medium- grained sandstone	335	51.3	25.7	100.2	103.42	77.57	12.93	12.93	14.77
11	Medium- grained conglomerate	373	23.7	11.9	74.6	47.78	35.83	8.36	3.58	6.83
12	Coarse-grained sandstone	437	10.9	5.5	62.7	21.97	17.58	1.32	3.08	2.44
13	Siltstone	737	16.4	8.2	57.3	33.06	28.93	1.24	2.89	3.67
14	Medium- grained sandstone	355	18.5	9.3	49.1	37.30	27.97	4.66	4.66	5.33
15	Siltstone	355	19.2	9.6	39.8	38.71	33.87	1.45	3.39	5.53
16	Coarse-grained sandstone	437	29	14.5	30.2	58.46	46.77	3.51	8.18	6.50
17	Sandy mudstone	673	13.6	6.8	15.7	27.42	23.50	2.74	1.18	3.05
18	Coal	473	5.7	2.9	8.9	11.49	9.19	1.61	0.69	1.28
19	Sandy mudstone	673	7.5	3.8	6.1	15.12	12.96	1.51	0.65	1.68
20	Coarse-grained sandstone	437	4.6	2.3	2.3	9.27	7.42	0.56	1.30	1.03
SUM	_	_	415.8	207.9		838.25	676.47	76.63	85.14	104.81

layers, and ultimately roof collapse. The overlying strata movement and spatial structure evolution induced by coal mining are illustrated in Figure 5.

Following the formation of the initial cut, continuous advancement of the working face resulted in a cantilevered roof over the subsequent space. When the face advanced to 50 m, micro-

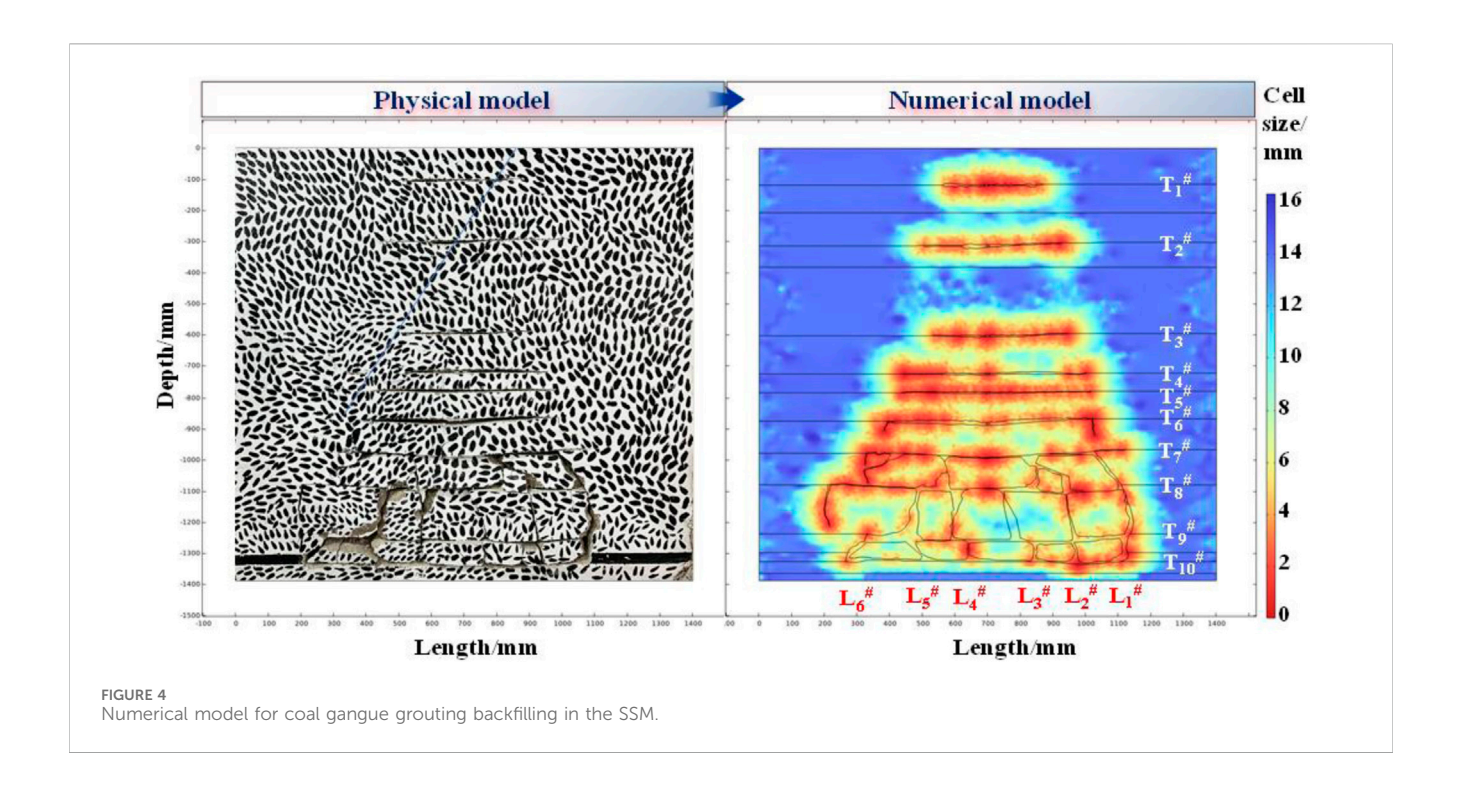


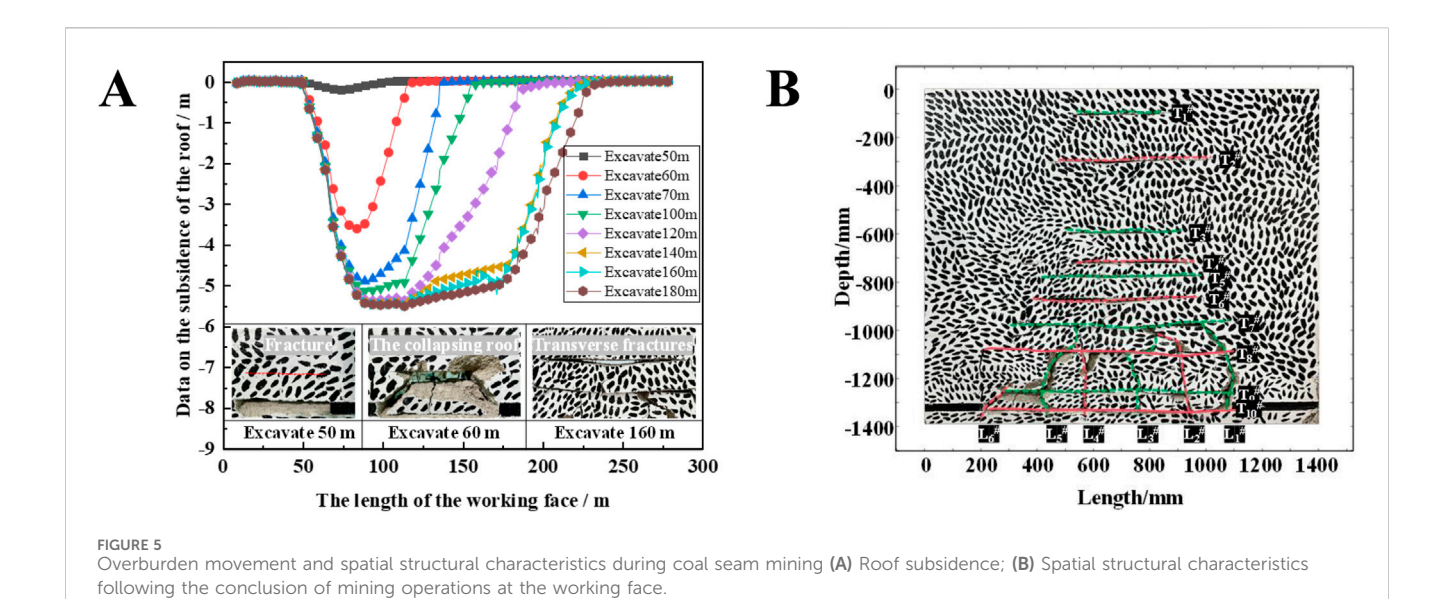
TABLE 4 Design of the simulation solution.

Scheme	Grouting pressure/MPa	Grouting layer/#	Grout concentration/%
1	0.4	T ₁ *- T ₃ *	70
2	0.4	T ₁ *- T ₆ *	60
3	0.4	T ₁ *- T ₁₀ *, L ₁ *- L ₆ *	65
4	0.6	T ₁ *- T ₃ *	60
5	0.6	T ₁ *- T ₆ *	65
6	0.6	T ₁ *- T ₁₀ *, L ₁ *- L ₆ *	70
7	0.8	T ₁ *- T ₃ *	65
8	0.8	T ₁ *- T ₆ *	70
9	0.8	T ₁ *- T ₁₀ *, L ₁ *- L ₆ *	60

fractures developed in the roof strata, as shown in Figure 5A. These micro-fractures represent the roof's response to stress redistribution. The roof subsidence curve exhibited a slight concave deformation, though the overall subsidence trend remained minimal, with a maximum displacement of only 0.20 m. As the working face reached 60 m, the load on the roof exceeded its bearing capacity, leading to fracture of the roof strata and the first occurrence of significant roof weighting. The subsidence curve showed a pronounced concave shape, indicating a clear and accelerated subsidence trend, with the maximum displacement reaching 3.60 m. During the face advancement from 100 m to 180 m, the structural evolution of the SSM exhibited varying characteristics at different stages. At 100 m, separation layer intensified, reflecting increased differential deformation and enhanced separation between roof layers as mining progressed. The shape of the subsidence curve transitioned from a "V" to a "U" shape, with

displacement reaching 5.15 m. Between 120 m and 160 m of advancement, the "U"-shaped subsidence curve gradually elongated, with displacements increasing from 5.39 m to 5.49 m. Strata movement remained relatively stable during this stage, indicating that the roof had reached a temporary equilibrium state. Although separation layer persisted, its progression slowed. By the time the working face advanced to 180 m, the displacement reached 5.51 m, and separation layer continued to diminish. This suggests that with further face advancement, the roof experienced a series of deformations that partially mitigated interlayer separation, thereby enhancing overall roof stability. Ultimately, a stable fracture network consisting of 10 transverse $(T_1^*-T_{10}^*)$ and 6 longitudinal $(L_1^*-L_6^*)$ fracture zones was formed.

In summary, following the initial roof weighting and the emergence of separation layer, continued advancement of the working face exacerbates the development of separation layer.



-200 -200 -200 -400 -600 -600 -600 -800 -1000 -1000 -1000 -1200 -1200 -1200 -1400 600 800 1000 1200 1400 600 800 1000 1200 1400 600 800 1000 1200 1400 200 400 200 400 200 400 Length/mm Length/mm -200 -200 -400 -600 -600 -600 Depth/n Depth 908-Depti 008--1000 -1000 -1000 -1200 -1200 -1200 800 1000 1200 1400 600 800 1000 1200 1400 600 800 1000 1200 1400 200 400 600 200 400 200 400 Length/mm Length/mm Length/mm FIGURE 6 Spatiotemporal distribution of slurry during grouting.

This process aggravates roof instability and leads to a more complex mechanical state of the roof. When stresses exceed critical levels, roof failure occurs, accompanied by the formation of separation layer in the overlying strata. Consequently, the evolutionary pattern of separation layer can be described as follows: as the working face advances, the fracture structure of the overlying strata progressively

propagates upward, and separation layer initiation shifts to higher levels. With further face advancement, interlayer separation is partially mitigated, leading to improved roof stability. Ultimately, a stable fracture network consisting of 10 transverse and 6 longitudinal fracture zones forms in the SSM. Among these, the fracture network formed by $T_7^\#$ to $T_{10}^\#$ and $L_1^\#$ to $L_6^\#$

constitutes the key SSM within the SSM for accommodating slurry and achieving effective backfilling.

3.2 Spatiotemporal evolution of coal gangue slurry flow and diffusion in the SSM

Based on the real-time photographic records of coal gangue slurry diffusion at different time intervals, the flow and diffusion state of the slurry within the SSM over a 30-second grouting period was plotted, as shown in Figure 6.

Based on real-time images of coal gangue slurry diffusion at different time intervals, the flow and diffusion patterns within the SSM over the 30-second grouting period were plotted, as shown in Figure 6. As grouting time increased, the diffusion range of the coal gangue slurry progressively expanded. Fractures provided dominant flow paths, with the slurry preferentially propagating along these fissures. The filled area gradually increased, extending from localized near-field regions to a broader fracture network in the far field. During the initial grouting stage, the slurry was mainly concentrated near the grouting hole, with limited diffusion. Within the first 6 s, the slurry initially appeared on the right side of $T_3^{\#}$, $T_4^{\#}$, $T_5^{\#}$, and $T_6^{\#}$, then spread toward the left side of $T_3^{\#}$ and $T_4^{\#}$, while flow in $T_5^{\#}$ and T₆[#] remained predominantly rightward. By 12 s, the slurry further extended into the surrounding far-field fracture network, advancing along both horizontal and vertical fractures and beginning to enter the subsequent space. Inside the subsequent space, the overall flow trend was "top-to-bottom" and "right-to-left," with a faster diffusion rate through fracture zones within the subsequent space compared to those in the upper sections. With continued grouting, the slurry propagated past large broken rocks and permeated into smaller fractures and the caved zone, forming a more extensive distribution in the middle and bottom fracture networks. Subsequently, as the near-field slurry began to set and grouting pressure attenuated in the far field, the diffusion distance per unit time gradually decreased. This was particularly evident in ${T_1}^{\#}-{T_6}^{\#}$ above the subsequent space. By the 30-s mark, a relatively continuous distribution zone of coal gangue slurry had formed in the model, achieving sufficient diffusion in both horizontal and vertical fractures and largely filling the main fracture network, indicating effective grouting performance.

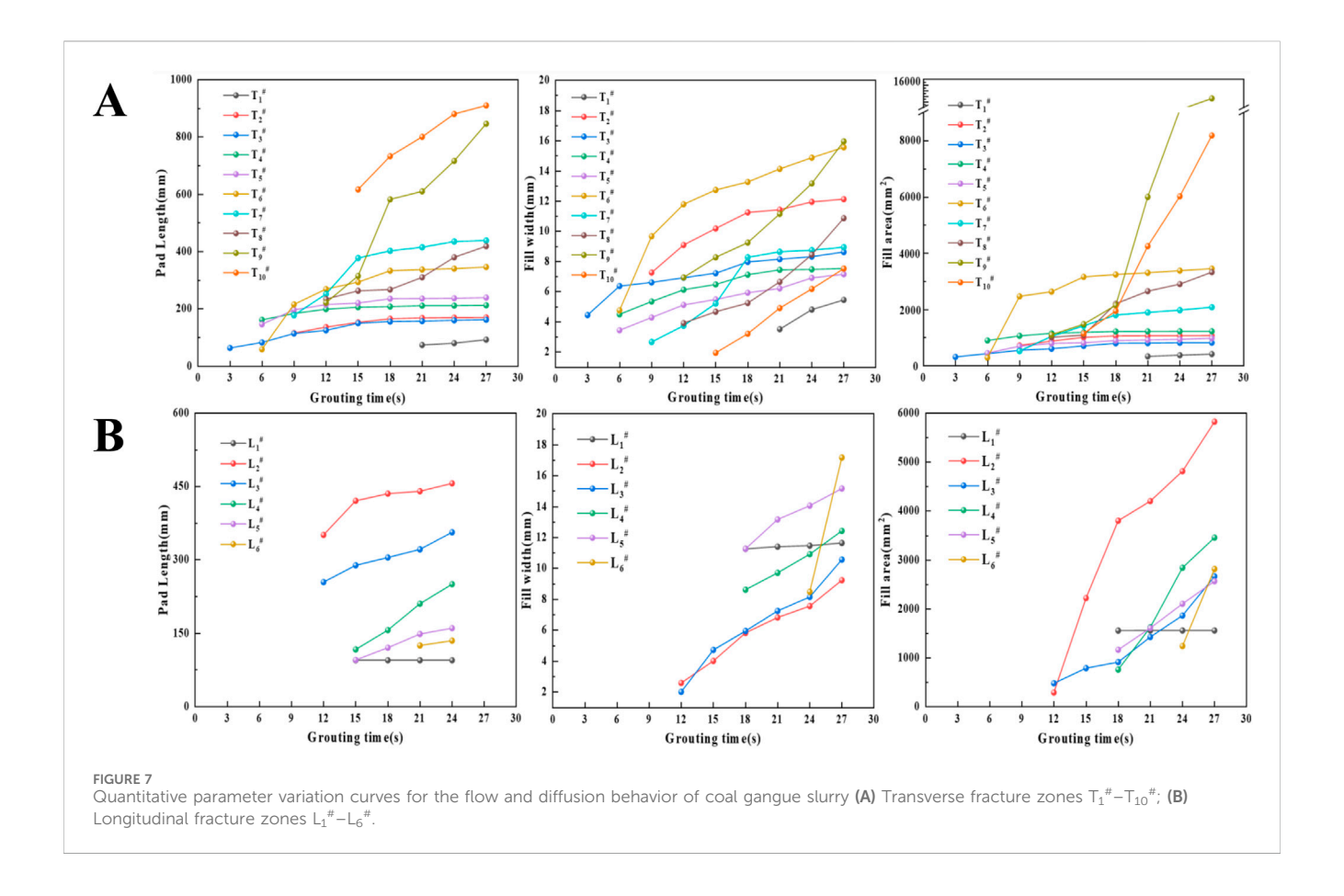
The grouting results in the SSM can be categorized into filled and unfilled zones. $T_1^\#$ - $T_6^\#$ above the subsequent space were fully filled, with the slurry exhibiting a "spindle-shaped" diffusion pattern (greater filling height in the center, tapering toward both sides). Additionally, elliptical unfilled areas were observed in some fracture zones due to the presence of air pockets, which prevented complete filling. At the bottom of the subsequent space, most fracture zones were fully filled, but the longitudinal fractures on both sides remained unfilled. In particular, the upper-left section of the subsequent space contained unfilled zones, attributable to factors such as slurry pressure, flow rate, and fracture connectivity. Therefore, well-connected fracture zones served as effective diffusion pathways, allowing rapid slurry penetration, whereas narrow or sealed fractures hindered slurry entry, resulting in ineffective diffusion paths. In light of this phenomenon, particular attention should be paid to the following measures in engineering applications: (1) Use pre-grouting ventilation or install exhaust pipes at potential air trap sites to promote air escape. (2) Optimize grouting pressure and flow rate, potentially employing pulsed grouting techniques to help displace trapped air. (3) Enhance fracture connectivity by optimizing grouting hole layout based on prior knowledge of the fracture network. These steps can significantly improve the efficiency and effectiveness of grouting operations.

In summary, as grouting time increases, the diffusion range of coal gangue slurry continues to expand. Initially, the slurry propagates preferentially along major fractures, then progressively fills the subsequent space and penetrates into the surrounding fracture network, ultimately forming a continuous backfilled distribution zone. Furthermore, the diffusion of coal gangue slurry is predominantly governed by the connectivity of fracture zones. Well-connected fractures serve as effective diffusion pathways, whereas narrow or sealed fractures result in ineffective paths. Additionally, localized air pockets can lead to unfilled voids. Therefore, during field grouting operations, attention must be paid to venting air from the SSM to ensure effective filling.

3.3 Variation in quantitative parameters of coal gangue slurry diffusion behavior in the SSM

To further quantitatively analyze the flow and diffusion behavior of coal gangue slurry in the SSM, quantitative parameters including the diffusion length, width, and area within each fracture zone over different grouting time intervals were derived based on visualized slurry diffusion pathways, as shown in Figure 7.

The study revealed that grout diffusion occurs sequentially, with certain separated layers acting as preferential or disadvantaged grouting zones. At 3 s and 6 s of grouting, no coal gangue grout was detected in $T_1^{\#}$ and $T_2^{\#}$. However, in the subsequent grouting stages, the diffusion length and filling area of the coal gangue grout continued to increase, albeit at a relatively low growth rate. In T₃*, at 3 s, the diffusion length and filled area reached 63.72 mm and 320.40 mm², respectively. By 27 s, these values increased to 162.15 mm and 824.16 mm², representing growth rates of approximately 154.47% and 157.40%. T₄[#] and T₅[#] consistently showed relatively slow diffusion rates throughout the grouting process. For T₆[#], at 6 s, the diffusion length and filled area were 59.22 mm and 294.54 mm². By 27 s, these measurements rose significantly to 345.96 mm and 3,456.45 mm², corresponding to increases of about 484.19% and 1,077.2%. Thus, in $T_1^{\#}-T_6^{\#}$ during the early grouting stage (3-9 s), coal gangue slurry diffused rapidly with high rates of area expansion. Over time, the diffusion rate gradually decreased as SSM within the fracture zones were progressively filled. Eventually, slurry diffusion reached a stable state, with the rate of area change leveling off. In T_7^* , at 9 s, the diffusion length and filled area were 178.02 mm and 528.57 mm². By 27 s, these values grew to 438.58 mm and 2084.16 mm², reflecting increases of approximately 146.37% and 294.30%. No slurry flow was observed in $T_8^{\#}$, $T_9^{\#}$, and $T_{10}^{\#}$ during the initial grouting phase. At 12 s, the diffusion lengths in $T_8^{\#}$ and $T_9^{\#}$ were 234.42 mm and 221.58 mm, respectively, while $T_{10}^{\#}$ reached 616.45 mm at 15 s. By the end of grouting, the filled areas for these three zones were 3,329.64 mm², 15,317.16 mm², and 8,179.60 mm², respectively,



indicating that $T_9^\#$ exhibited the most effective slurry diffusion. Finally, $L_1^\#$ contained narrow fractures and showed minimal diffusion after initial slurry detection, classifying it as an ineffective path. In contrast, $L_2^\#-L_6^\#$ demonstrated rapid diffusion upon first observation. $L_2^\#$ served as a dominant flow path, with its filled area increasing from 291.95 mm² at 12 s to 5,820.01 mm² at 27 s—a growth of approximately 1893.50%.

In summary, the quantitative parameters of diffusion behavior in zones T₁*-T₆* above the subsequent space exhibit a pattern of rapid initial increase followed by stabilization. That is, as grouting time progresses, the diffusion range of the coal gangue slurry continues to extend outward, showing a non-linear growth trend, but with a gradually decreasing growth rate until the curve flattens. In contrast, the diffusion parameters in zones $T_7^{\#}$ - $T_{10}^{\#}$ within the subsequent space and L₁*-L₆* demonstrate a pattern of rapid increase without reaching a stable state. Therefore, the stabilization of coal gangue slurry diffusion in areas more significantly affected by mining activities lags behind that in less affected areas. This is because the fracture space formed by the collapse of the immediate roof and main roof after the working face has been excavated is substantially larger than other fractures. As a result, regions more affected by mining allow for a much larger diffusion range of coal gangue slurry and can store a greater volume of slurry. Thus, under constant grouting pressure, there exists a limiting diffusion radius. Once the diffusion radius of the coal gangue slurry approaches this limit, further grouting becomes increasingly difficult. Consequently, in field grouting operations, the spacing between multiple grouting pipelines can be determined based on this limiting diffusion radius.

4 Discussion

4.1 Physical similarity model and numerical simulation model validation results

The numerical simulation results at 24 s of grouting were compared with the physical simulation to validate the accuracy of the numerical model. A comparison between the physical and numerical simulation results is shown in Figure 8.

Analysis of Figure 8 indicates that at 24 s of grouting, the diffusion ranges of coal gangue slurry obtained from the physical and numerical simulations are consistent. Furthermore, the variation trends of diffusion length in fractures $T_1^\#-T_6^\#$ obtained by both methods at different grouting times are essentially identical: both show a rapid increase followed by stabilization as grouting progresses. At 21 s and 27 s of grouting, the differences in diffusion length in $T_1^\#-T_6^\#$ between the two methods are 0.74 mm, 0.93 mm, 1.68 mm, 1.70 mm, 1.57 mm, 1.62 mm and 2.11 mm, 2.12 mm, 2.36 mm, 2.40 mm, 3.37 mm, 3.46 mm, respectively. The corresponding error range is only 1.4%–5.5%, indicating a high level of agreement.

In summary, the strong agreement between the two methods in characterizing the diffusion behaviour of coal gangue slurry within

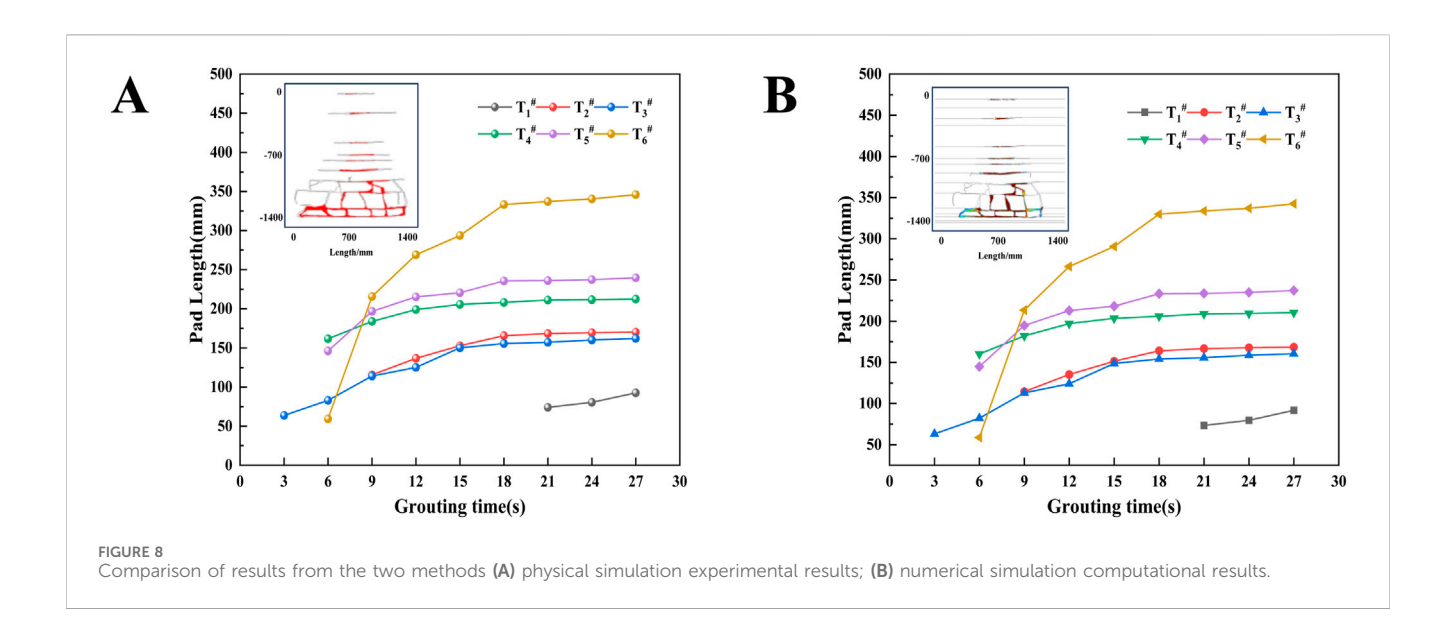


TABLE 5 Orthogonal test results for factors affecting coal gangue slurry diffusion.

	3		3 3 3		
Scheme	Grouting pressure/MPa	Grouting layer/#	Grout concentration/%	Cumulative length at 15s $L_{\text{total-15 s}}$ /mm	Cumulative length at 30s $L_{\rm total-30~s}/{\rm mm}$
1	0.4	T ₁ *- T ₃ *	70	225.92	412.44
2	0.4	T ₁ #- T ₆ #	60	563.43	1,415.55
3	0.4	T ₁ *- T ₁₀ *, L ₁ *- L ₆ *	65	1,239.39	2,496.76
4	0.6	T ₁ *- T ₃ *	60	284.97	580.68
5	0.6	T ₁ *- T ₆ *	65	783.77	1,488.61
6	0.6	T ₁ *- T ₁₀ *, L ₁ *- L ₆ *	70	1897.4	3,448.4
7	0.8	T ₁ *- T ₃ *	65	415.48	713.65
8	0.8	T ₁ *- T ₆ *	70	1,014.93	1953.87
9	0.8	T ₁ *- T ₁₀ *, L ₁ *- L ₆ *	60	2,522.96	4,377.86

the SSM confirms the appropriateness of the numerical model's computational module selection. It also validates that the model parameters and boundary conditions are consistent with physical reality. Consequently, the numerical model developed in this study can be reliably utilized to analyse the diffusion patterns of coal gangue slurry under various grouting process parameters, thereby providing theoretical guidance for field applications.

4.2 Diffusion law of coal gangue slurry in the SSM under different grouting parameters

4.2.1 Comprehensive analysis of orthogonal test results

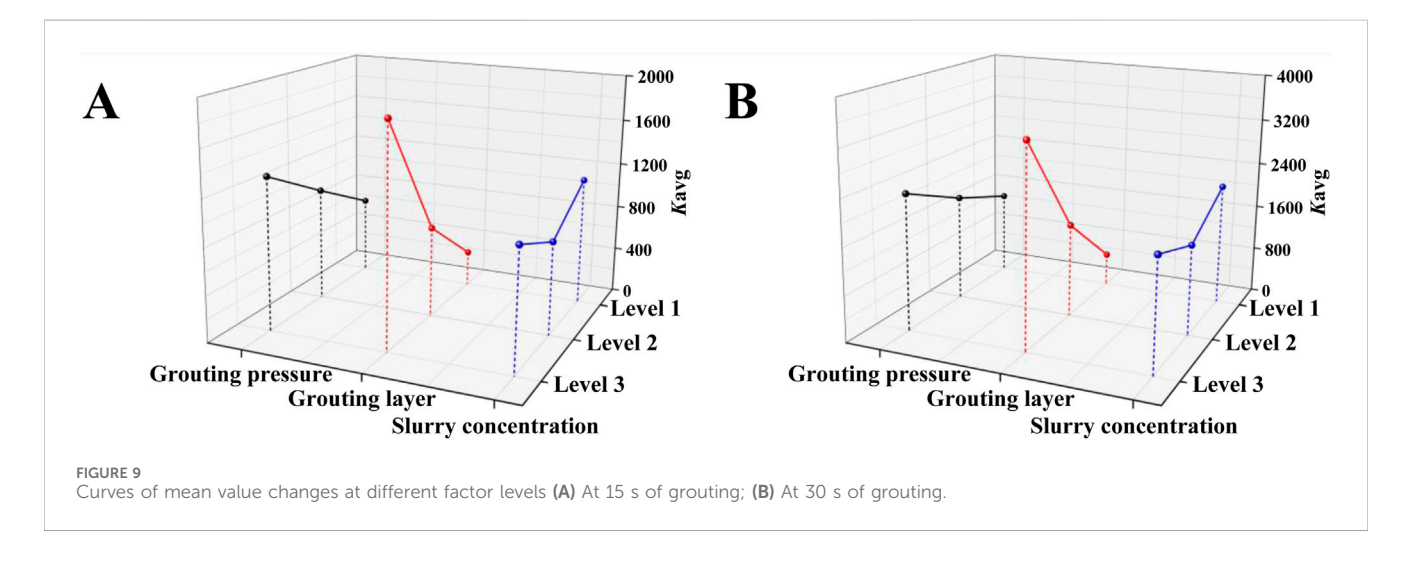
Building upon the preceding analysis, diffusion length has been identified as a comprehensive indicator for evaluating the diffusion behavior of coal gangue slurry. Therefore, this study adopts cumulative diffusion length—specifically the cumulative length at 15 s ($L_{\rm total-15s}$) and at 30 s ($L_{\rm total-30s}$) of grouting—as the

evaluation metric to analyze the influence of different grouting process parameters on slurry diffusion. Using orthogonal experimental design, the effects of grouting pressure, grouting horizon, and slurry concentration on cumulative diffusion length were investigated. The orthogonal test results are presented in Table 5.

Analysis of Table 5 shows that the minimum values of $L_{\rm total-15s}$ and $L_{\rm total-30s}$ under different grouting process parameters are 225.92 mm and 412.44 mm, respectively, while the maximum values are 2,522.96 mm and 4,377.86 mm. This indicates a reasonable range of variation for both $L_{\rm total-15s}$ and $L_{\rm total-30s}$, confirming that the selected factor levels are appropriate. Furthermore, grouting pressure and grouting horizon have a significant influence on the diffusion behavior of coal gangue slurry (as reflected by $L_{\rm total-15s}$ and $L_{\rm total-30s}$). Higher pressure and a broader grouting horizon promote greater diffusion of the coal gangue slurry. In contrast, within the tested range, the concentration of the coal gangue slurry exhibits a relatively minor effect on diffusion length. Nevertheless, it is important to note that while

TABLE 6 Range analysis.

ltem		Level	Factor 1 (Grouting pressure)	Factor 2 (Grouting layer)	Factor 3 (Grout concentration)	
Grouting 15s	ing 15s K 1		2028.74	926.37	3,371.36	
		2	2,966.14	2,362.13	2,438.64	
		3	3,953.37	5,659.75	3,138.25	
	E	Best level	3	3	1	
		R	641.54	1,577.79	310.91	
		orizontal quantity	3	3	3	
	Number of replicates per level <i>r</i>		3.0	3.0	3.0	
Grouting 30s	K	1	4,324.75	1706.77	6,374.09	
	2		5,517.69	4,858.03	4,699.02	
		3	7045.38	10,323.02	5,814.71	
	Best level R Horizontal quantity		3	3	1	
			906.88	2,872.08	558.36	
			3	3	3	
	rep	umber of licates per level <i>r</i>	3.0	3.0	3.0	



slurry concentration has the least impact on the diffusion range, using excessively high concentrations can lead to practical engineering challenges such as increased pumping resistance, potential pipeline blockage, and difficulties in long-distance transportation. Therefore, although its influence on the diffusion distance is relatively minor, the selection of slurry concentration remains a critical consideration for ensuring the smooth implementation of grouting operations in the field. Therefore, in field grouting operations, adjusting the grouting pressure and selecting an appropriate grouting horizon should be prioritized to enhance the diffusion effectiveness of coal gangue slurry.

4.2.2 Influence of different grouting process parameters on $L_{\text{total-15s}}$ and $L_{\text{total-30s}}$

Range analysis was applied to evaluate the orthogonal experimental data. This method can be used to identify dominant factors and compare the performance of different factor levels. The range analysis results for $L_{\rm total-15s}$ and $L_{\rm total-30s}$ at 15 s and 30 s of grouting, along with the mean value variation curves for each factor level, are presented in Table 6 and Figure 9, respectively.

The study revealed that at 15 s of grouting, the range (R) for grouting pressure was 641.54, indicating a moderate influence on

 $L_{\text{total-15s}}$. As the grouting pressure increased from 0.4 MPa to 0.8 MPa, the K_{avg} value rose from 676.25 to 1,317.79, suggesting that appropriately increasing grouting pressure can enhance the diffusion range of coal gangue slurry to some extent. The range for grouting horizon was 1,577.79, demonstrating the most significant impact on $L_{\text{total-15s}}$. The K_{avg} values for levels 1, 2, and 3 were 306.79, 787.38, and 1886.58, respectively, showing a substantial increasing trend. Selecting level 3 of the grouting horizon had the greatest positive effect on coal gangue slurry diffusion. The range for coal gangue slurry concentration was 310.91, indicating a relatively weak influence on $L_{\text{total-15s}}$. The K_{avg} values for levels 1, 2, and 3 were 1,123.79, 812.88, and 1,046.08, respectively, with minor variations. This suggests that adjusting the slurry concentration within a certain range has limited effect on improving the diffusion range. At 30 s of grouting, the range for grouting pressure was 906.88. As the pressure increased from level 1 to level 3, the K_{avg} value grew from 1,441.58 to 2,348.46, showing a notable increase and confirming a significant influence on $L_{\text{total-30s}}$. The range for grouting horizon was 2,872.08. The K_{avg} value increased dramatically from 568.92 at level 1 to 3,441.01 at level 3, underscoring that the grouting horizon has the most prominent effect on $L_{\text{total-30s}}$ and is the key factor governing coal gangue slurry diffusion. The range for slurry concentration was 558.36. The K_{avg} value decreased from 2,124.70 at level 1 to 1938.24 at level 3, with a relatively small overall reduction. This indicates that slurry concentration has a certain but limited influence on $L_{\text{total-30s}}$.

In summary, the grouting horizon is the most dominant factor influencing the diffusion range of coal gangue slurry. As the grouting horizon increases, the $K_{\rm avg}$ value shows a rapid upward trend, indicating that elevating its level significantly enhances grouting effectiveness. Grouting pressure is the second most influential factor. With increasing pressure, the $K_{\rm avg}$ value exhibits a clear rising trend, demonstrating that higher pressure markedly promotes the diffusion of coal gangue slurry. In contrast, the concentration of coal gangue slurry has a relatively weak effect. As concentration increases, the $K_{\rm avg}$ value initially decreases and then rises, with both $L_{\rm total-15s}$ and $L_{\rm total-30s}$ reaching their maximum values at the first concentration level. Consequently, the optimal levels for the three factors are Level 3, Level 3, and Level 1, corresponding to a grouting pressure of 0.8 MPa, a comprehensive grouting horizon, and a coal gangue slurry concentration of 60%.

5 Conclusions and future work

5.1 Main conclusion

This study comprehensively investigated the flow and diffusion behavior of coal gangue slurry in the SSM through integrated physical and numerical simulations. The main conclusions are as follows:

 The advancement of the working face drives the dynamic evolution of the overburden, which sequentially undergoes stages of micro-fracture initiation, separation layer development, and structural collapse. This process culminates in the formation of a stable fracture network architecture within the Subsequent Space after Mining

- (SSM), comprising 10 transverse $(T_1^\#-T_{10}^\#)$ and 6 longitudinal $(L_1^\#-L_6^\#)$ fracture zones. The interconnected network formed by zones $T_7^\#-T_{10}^\#$ and $L_1^\#-L_6^\#$ characterized by its superior volume capacity and connectivity, is identified as the key SSM for effectively accommodating backfill slurry and controlling subsidence.
- 2. The flow and diffusion of coal gangue slurry within the SSM exhibit significant spatiotemporal differentiation, primarily governed by the heterogeneity of the fracture network. In the upper fracture zones $T_1^*-T_6^*$, slurry diffusion presents a distinct "oval-spindle" morphology, with the rate progressively declining over time as the available fracture space is filled. In contrast, within the key SSM zones $(T_7^*-T_{10}^*)$ and $L_1^*-L_6^*)$, slurry migrates in a sustained "top-to-bottom" and "right-to-left" pattern without observable deceleration, indicating a larger storage capacity and more dominant flow paths.
- 3. The grouting horizon is the primary factor affecting the diffusion range of coal gangue slurry. As it expands, the $K_{\rm avg}$ value rises sharply, indicating significantly improved grouting effectiveness. Grouting pressure is the secondary factor, with $K_{\rm avg}$ showing a clear upward trend as pressure increases. Slurry concentration has the weakest impact; $K_{\rm avg}$ decreases initially then increases with concentration, while both $L_{\rm total-15s}$ and $L_{\rm total-30s}$ peak at the lowest concentration. The optimal parameters are: 0.8 MPa grouting pressure, comprehensive grouting horizon, and 60% slurry concentration. In engineering applications, to enhance grouting effectiveness, it is recommended to employ preventilation for air removal, optimize pressure/flow rates in conjunction with pulsed grouting, and improve fracture connectivity through optimized borehole layout.

5.2 Future work

Research on the flow and diffusion behavior of coal gangue slurry in SSM is of significant importance for the disposal of coal-based solid waste and the prevention of ground subsidence. However, for the future engineering application of this technology, the following critical practical issues must be systematically addressed through research:

- Grout leakage mechanisms in mined-out areas: Through systematic analysis of grout leakage cases and physical simulations, this work summarizes leakage modes and characteristics, revealing the formation of leakage channels and grout loss mechanisms in areas affected by overburden separation.
- 2. Impact of grouting backfill on mine water environment: Using triaxial rock seepage tests and a self-developed multi-field leaching device, this study evaluates changes in permeability of grouted rock masses and assesses the leaching behavior of heavy metals and pH evolution in slurry, clarifying potential impacts of grouting on mine water quality.
- 3. Formation mechanism and stability of regenerated overburden via grouting: By analyzing macro-mechanical properties and micro-structures of grout materials and coal-rock composites,

along with spectroscopic analysis of hydration products, this research elucidates the regeneration mechanism of damaged overburden. An equivalent filling rate-based mechanical model is established to derive instability criteria and evolution patterns during grouting, leading to a stability control framework for regenerated structures.

Data availability statement

The original contributions presented in the study are included in the article/supplementary material, further inquiries can be directed to the corresponding authors.

Author contributions

HL: Writing – original draft, Funding acquisition, Writing – review and editing. JG: Data curation, Writing – original draft. AR-D: Writing – review and editing. ET: Writing – review and editing. JF: Software, Writing – original draft. XL: Validation, Writing – original draft. XW: Funding acquisition, Writing – review and editing. HZ: Writing – review and editing.

Funding

The authors declare that financial support was received for the research and/or publication of this article. This work was funded by the National Natural Science Foundation of China (No. 52404154), the Postdoctoral Fellowship Program of China Postdoctoral Science

References

Amiri, H., Azadi, S., Karimaei, M., Sadeghi, H., and Dabbaghi, F. (2022). Multi-objective optimization of coal waste recycling in concrete using response surface methodology. *J. Build. Eng.* 45, 103472. doi:10.1016/j.jobe.2021.103472

Bouchelaghem, F., and Vulliet, L. (2001). Mathematical and numerical filtration–advection–dispersion model of miscible grout propagation in saturated porous media. *Int. J. Numer. Anal. Meth. Geomech.* 25, 1195–1227. doi:10.1002/nag.173

El Mohtar, C., Jaffal, H., Miller, A. K., and Ward, K. (2022). Implementing digital imaging for improved understanding of microfine cement grout permeation and filtration. *Geotechnical Geol. Eng.* 40, 4473–4485. doi:10.1007/s10706-022-02164-z

El Tani, M., and Stille, H. (2017). Grout spread and injection period of silica solution and cement mix in rock fractures. *Rock Mech. Rock Eng.* 50, 2365–2380. doi:10.1007/s00603-017-1237-8

Gao, S., Zhang, S. M., and Guo, L. H. (2021). Application of coal gangue as a coarse aggregate in green concrete production: a review. *Materials* 14, 6803. doi:10.3390/ma14226803

Ghabraie, B., Ren, G., Zhang, X. Y., and Smith, J. (2015). Physical modelling of subsidence from sequential extraction of partially overlapping longwall panels and study of substrata movement characteristics. *Int. J. Coal Geol.* 140, 71–83. doi:10.1016/j.coal.2015.01.004

Ghabraie, B., Ghabraie, K., Ren, G., and Smith, J. V. (2017). Numerical modelling of multistage caving processes: insights from multi-seam longwall mining-induced subsidence. *Int. J. Numer. Anal. Methods Geomechanics* 41, 959–975. doi:10.1002/nag.2659

Güllü, H. (2016). Comparison of rheological models for jet grout cement mixtures with various stabilizers. *Constr. Build. Mater.* 127, 220–236. doi:10.1016/j.conbuildmat. 2016.09.129

Foundation (No. GZC20233012), Key Laboratory of Xinjiang Coal Resources Green Mining, Ministry of Education (No. KLXGY-KB2412), the Natural Science Foundation of Jiangsu Province (No. BK20210501), China National Administration of Coal Geology Major Special Project (No. ZMKJ-2023-JBGS02) the 111 Project (No. B21016).

Conflict of interest

The authors declare that the research was conducted in the absence of any commercial or financial relationships that could be construed as a potential conflict of interest.

Generative AI statement

The authors declare that no Generative AI was used in the creation of this manuscript.

Any alternative text (alt text) provided alongside figures in this article has been generated by Frontiers with the support of artificial intelligence and reasonable efforts have been made to ensure accuracy, including review by the authors wherever possible. If you identify any issues, please contact us.

Publisher's note

All claims expressed in this article are solely those of the authors and do not necessarily represent those of their affiliated organizations, or those of the publisher, the editors and the reviewers. Any product that may be evaluated in this article, or claim that may be made by its manufacturer, is not guaranteed or endorsed by the publisher.

Heever, E. M., Sutherland, A. P. N., and Haldenwang, R. (2014). Influence of the rheological model used in pipe-flow prediction techniques for homogeneous Non-Newtonian fluids. *J. Hydraulic Eng.* 140, 04014059. doi:10.1061/(ASCE)HY.1943-7900. 0000934

Karimaei, M., Dabbaghi, F., Sadeghi-Nik, A., and Dehestani, M. (2020). Mechanical performance of green concrete produced with untreated coal waste aggregates. *Constr. Build. Mater.* 233, 117264. doi:10.1016/j.conbuildmat.2019.117264

Khanal, M., Adhikary, D., Jayasundara, C., and Balusu, R. (2016). Numerical study of mine site specific multi seam mining and its impact on surface subsidence and chain pillar stress. *Geotechnical Geol. Eng.* 34, 217–235. doi:10.1007/s10706-015-9940-2

Kostecki, T., and Spearing, A. J. S. (2015). Influence of backfill on coal pillar strength and floor bearing capacity in weak floor conditions in the Illinois Basin. *Int. J. Rock Mech. Min.* 76, 55–67. doi:10.1016/j.ijrmms.2014.11.011

Lazorenko, G., and Kasprzhitskii, A. (2025). Resource utilization of coal gangue through geopolymerization: unraveling trends, gaps, and circular economy insights. *Sustain. Chem. One World.* 8, 100142. doi:10.1016/j.scowo.2025.100142

Letelier, M. F., Siginer, D. A., and González, E. (2023). On the flow of viscoelastic fluids in non-circular tubes. *Int. J. Non-Linear Mech.* 153, 104408. doi:10.1016/j.ijnonlinmec.2023.104408

Li, G. S. (2023). "Coupling mechanism and coordination technology of underground coal mining and mine reclamation in coal-grain overlapping areas of Eastern China," in *Ph.D. thesis, China university of mining and technology* (Xuzhou, China). doi:10.27623/d.cnki.gzkyu.2023.000066

Li, J. Y., and Wang, J. M. (2019). Comprehensive utilization and environmental risks of coal gangue: a review. *J. Clean. Prod.* 239, 117946. doi:10.1016/j.jclepro.2019. 117946

Li, X. B., He, W. R., and Xu, Z. H. (2020). Study on law of overlying strata breakage and migration in downward mining of extremely close coal seams by physical similarity simulation. *Adv. Civ. Eng.* 11, 2898971. doi:10.1155/2020/2898971

Mohajerani, S., Baghbanan, A., Wang, G., and Forouhandeh, S. F. (2017). An efficient algorithm for simulating grout propagation in 2D discrete fracture networks. *Int. J. Rock Mech. Min. Sci.* 98, 67–77. doi:10.1016/j.ijrmms.2017.07.015

- Pedrotti, M., Wong, C., El Mountassir, G., and Lunn, R. J. (2017). An analytical model for the control of silica grout penetration in natural groundwater systems. *Tunn. Undergr. Space Technol.* 70, 105–113. doi:10.1016/j.tust.2017.06.023
- Qu, W. Y., Chen, J., Li, Z., Luo, M., Lu, H. X., Hu, X. G., et al. (2022). Rheological modeling and simulation of semi-solid slurry based on experimental study. *Scr. Mater.* 220, 114932. doi:10.1016/j.scriptamat.2022.114932
- Sahoo, S. K., Behera, B., Yadav, A., Singh, G. S. P., and Sharma, S. K. (2020). Plane-strain modeling of progressive goaf compaction in a depillaring working. *J. Institution Eng. (India)* 101, 233–245. doi:10.1007/s40033-020-00233-2
- Sepehri, M., Apel, D. B., and Hall, R. A. (2017). Prediction of mining-induced surface subsidence and ground movements at a Canadian diamond mine using an elastoplastic finite element model. *Int. J. Rock Mech. Min.* 100, 73–82. doi:10.1016/j.ijrmms.2017.
- Snehasree, N., Nuruddin, M., and Moghal, A. A. B. (2025). Critical appraisal of coal gangue and activated coal gangue for sustainable engineering applications. *Appl. Sci.* 15, 9649. doi:10.3390/app15179649
- Song, W., Zhang, J., Li, M., Yan, H., Zhou, N., Yao, Y., et al. (2022). Underground disposal of coal gangue backfill in China. *Appl. Sci.* 12, 12060. doi:10.3390/app122312060
- Taha, Y., Benzaazoua, M., Hakkou, R., and Mansori, M. (2017). Coal mine wastes recycling for coal recovery and eco-friendly bricks production. *Miner. Eng.* 107, 123–138. doi:10.1016/j.mineng.2016.09.001
- Tang, T., Wang, Z., Chen, L. Z., Wu, S., and Liu, Y. S. (2024). Opportunities, challenges and modification methods of coal gangue as a sustainable soil conditioner—A review. *Environ. Sci. Pollut. Res.* 31, 58231–58251. doi:10.1007/s11356-024-34895-2

- Wang, C. G., Wang, L. L., Song, Z. Q., and Pan, Y. L. (2004). Testing study on 3D similar material simulation for shallow coal seam mining. *Chin. J. Rock Mech. Eng.* S2, 4926–4929. (in Chinese). doi:10.3321/j.issn:1000-6915.2004.z2.045
- Wang, J., Ma, J., Yang, K., Yang, S. Y., and Shi, X. Y. (2021). Effects and laws analysis for the mining technique of grouting into the overburden bedding separation. *J. Clean. Prod.* 288, 125121. doi:10.1016/j.jclepro.2020.125121
- Wang, P. C., Yan, X. S., Sun, X. L., Liu, Z. Y., Duan, Y. Z., Ning, Z. W., et al. (2024). Permeation grouting mechanism of rapid-setting chemical grout considering spacetime variation of viscosity characteristics. *Rock Soil Mech.* 45, 12.
- Xu, Z. H., Li, Q. S., and Li, X. B. (2020). Overburden migration and failure characteristics in mining shallow buried coal seam with thick loose layer. Adv. Mater. Sci. Eng. 1, 9024751. doi:10.1155/2020/9024751
- Yavuz, H. (2004). An estimation method for cover pressure re-establishment distance and pressure distribution in the goaf of longwall coal mines. *Int. J. Rock Mech. Min. Sci.* 41, 193–205. doi:10.1016/S1365-1609(03)00082-0
- Yi, C., Ma, H. Q., Chen, H. Y., Wang, J. X., Li, Z. H., and Yu, M. K. (2023). Preparation and characterization of coal gangue geopolymers. *Constr. Build. Mater.* 187, 318–326. doi:10.1016/j.conbuildmat.2018.07.220
- Yu, H., Jia, H. S., Liu, S. W., Liu, Z. H., and Li, B. Y. (2021). Macro and micro grouting process and the influence mechanism of cracks in soft coal seam. *Int. J. Coal Sci. Technol.* 8, 969–982. doi:10.1007/s40789-020-00404-2
- Zhang, Z. L., Shao, Z. S., Fang, X. B., and Liang, X. J. (2018). Research on the fracture grouting mechanism and PFC numerical simulation in loess. *Adv. Mater. Sci. Eng.* 2018, 4784762. doi:10.1155/2018/4784762
- Zhang, Z., Gui, L., Liao, D., Sun, K., Liang, S., Duan, H., et al. (2023). Advances in high-value utilization of fly ash from coal-fired power plants. *Energy Environ. Prot.* 37, 1–11. doi:10.20078/j.eep.20230701
- Zheng, Z., Li, S. C., and Liu, R. T. (2021). Analysis on structural characteristics of grout and rock distribution in complex geological mixtures after grouting reinforcement and its mechanical strength. *Rock Mech. Rock Eng.* 54, 3757–3782. doi:10.1007/s00603-021-02461-8
- Zhou, N., Zhang, J. X., Xu, J. F., Wang, H. D., Liu, S. X., Li, M., et al. (2025). Experimental study on the flow and diffusion laws of heterogeneous gangue slurry in mining space. *Rock Mech. Rock Eng.* 58, 2589–2605. doi:10.1007/s00603-024-04367-7